LAWRENCE
LIVERMORE
NATIONAL
LABORATORY

UCRL-TR-222335

Low-Frequency Electromagnetic Backscatter from Buried Tunnels

Kendall Casey, Hsueh-yuan Pao

June 22, 2006

This work was performed under the auspices of the U.S. Department of Energy by University of California, Lawrence Livermore National Laboratory under Contract W-7405-Eng-48.

Low-Frequency Electromagnetic Backscatter from Buried Tunnels

Kendall F. Casey and Hsueh-Yuan Pao
University of California
Lawrence Livermore National Laboratory

June 21, 2006

1 Introduction

This progress report is submitted under a contract between the Special Project Office of DARPA and Lawrence Livermore National Laboratory. The Project Manager at DARPA is Dr. Michael Zatman. Our purpose under this contract is to investigate interactions between electromagnetic waves and a class of buried targets located in multilayered media with rough interfaces.

In this report, we investigate three preliminary problems. In each case our specific goal is to understand various aspects of the electromagnetic wave interaction mechanisms with targets in layered media. The first problem, discussed in Section 2, is that of low-frequency electromagnetic backscattering from a tunnel that is cut into a lossy dielectric half-space. In this problem, the interface between the upper (free space) region and the lower (ground) region is smooth. The tunnel is assumed to be a cylindrical free-space region of infinite extent in its axial direction and with a diameter that is small in comparison to the free-space wavelength. Because its diameter is small, the tunnel can be modeled as a buried "wire" described by an equivalent impedance per unit length.

In Section 3 we extend the analysis to include a statistically rough interface between the air and ground regions. The interface is modeled as a random-phase screen. Such a screen reduces the coherent power in a plane wave that is transmitted through it, scattering some of the total power into an incoherent field. Our analysis of this second problem quantifies the reduction in the coherent power backscattered from the buried tunnel that is caused by the roughness of the air-ground interface.

The problem of low-frequency electromagnetic backscattering from two buried tunnels, parallel to each other but at different locations in the ground, is considered in Section 4. In this analysis, we wish to determine the conditions under which the presence of more than one tunnel can be detected via backscattering.

Section 5 concludes the report with a summary of the investigations discussed herein and recommendations for future work on problems of this class.

2 Electromagnetic Backscattering from a Tunnel in a Lossy Half-Space

We consider electromagnetic backscattering from a buried wire.[1] The wire is located in the half-space $z < 0$, in which the relative permittivity is ϵ_r. The wire is parallel to the y-axis and is located at position $x = 0, z = -d$. A perpendicularly-polarized plane electromagnetic wave is incident on the half-space from the free-space region $z > 0$. The incident electric field is (the time dependence $\exp(j\omega t)$ is assumed)

$$E_{yi}(x,z) = E_0 e^{-jk_0(x\sin\theta_i - z\cos\theta_i)} \tag{1}$$

in which θ_i denotes the angle of incidence with respect to the positive z-direction and k_0 is the free-space wavenumber. The electric field E_y transmitted into the lower medium is easily shown to be

$$E_{yt}(x,z) = T(\theta_i) E_0 e^{-jk_0(x\sin\theta_i - z\sqrt{\epsilon_r - \sin^2\theta_i})} \tag{2}$$

where the transmission coefficient $T(\theta_i)$ is

$$T(\theta_i) = \frac{2\cos\theta_i}{\cos\theta_i + \sqrt{\epsilon_r - \sin^2\theta_i}} \tag{3}$$

Next consider the electric field radiated into the upper free-space region by the filamentary current I_0 on a buried wire located at $(0, -d)$. Write the electric field in the upper and lower regions in terms of Fourier integrals as

$$E_{y>}(x,z) = \frac{I_0}{2\pi}\int_{-\infty}^{\infty} A(k_x) e^{-jk_x x - jk_{z0} z} dk_x \tag{4}$$

$$E_{y<}(x,z) = \frac{I_0}{2\pi}\int_{-\infty}^{\infty} e^{-jk_x x}\left[B(k_x)e^{jk_{zg}z} + C(k_x)e^{-jk_{zg}|z+d|}\right] dk_x \tag{5}$$

where $k_{z0} = \sqrt{k_0^2 - k_x^2}$ and $k_{zg} = \sqrt{k_0^2\epsilon_r - k_x^2}$; the functions $A(k_x)$ and $B(k_x)$ are to be determined. The function $C(k_x)$ is known; it is given by

$$C(k_x) = -\frac{k_0 Z_0}{2k_{zg}} \tag{6}$$

in which Z_0 denotes the intrinsic impedance of free space. The term involving $C(k_x)$ in the integral in eq. (5) above is the electric field directly radiated by the filamentary current, and the term involving $B(k_x)$ represents the field that is reflected back into the ground by the air-ground interface. We have

$$\frac{I_0}{2\pi}\int_{-\infty}^{\infty} e^{-jk_x x} C(k_x) e^{-jk_{zg}|z+d|} dk_x = -\frac{jk_0 Z_0 I_0}{4j} H_0^{(2)}(k_g \rho') \tag{7}$$

in which $k_g = k_0\sqrt{\epsilon_r}$ is the propagation constant in the lower medium and $\rho' = \sqrt{x^2 + (z+d)^2}$ denotes the distance from the wire axis to the observation point in the lower medium.

The tangential magnetic field component H_x is obtained from E_y via

$$H_x(x,z) = \frac{1}{jk_0 Z_0}\frac{\partial E_y}{\partial z} \tag{8}$$

[1] By "wire" we mean a cylindrical obstacle whose radius is small compared to the wavelength. It is not necessarily a perfect conductor.

Making E_y and H_x continuous at $z = 0$ and solving for $A(k_x)$ and $B(k_x)$, we obtain

$$A(k_x) = C(k_x)e^{-jk_{zg}d}\left(\frac{2k_{zg}}{k_{z0}+k_{zg}}\right) \tag{9}$$

$$B(k_x) = C(k_x)e^{-jk_{zg}d}\left(\frac{k_{zg}-k_{z0}}{k_{z0}+k_{zg}}\right) \tag{10}$$

so that the electric field radiated into the free-space region by the wire is

$$E_{y>}(x,z) = -\frac{k_0 Z_0 I_0}{2\pi}\int_{-\infty}^{\infty} e^{-jk_x x}e^{-jk_{zg}d-jk_{z0}z}\frac{dk_x}{k_{z0}+k_{zg}} \tag{11}$$

Now we evaluate the integral above in the far zone using the method of steepest descents. We find

$$E_{y>}(\rho,\theta) \sim -\frac{jk_0 Z_0 I_0}{\sqrt{8\pi jk_0\rho}}\,T(\theta)e^{-jk_0\rho-jk_0 d\sqrt{\epsilon_r-\sin^2\theta}} \tag{12}$$

The radiated power density, normalized by the incident power density, is given in the far zone by

$$\frac{S_r}{S_i} = k_0^2\left|\frac{Z_0 I_0}{E_0}\right|^2\frac{1}{8\pi k_0\rho}\left|T(\theta)e^{-jk_0 d\sqrt{\epsilon_r-\sin^2\theta}}\right|^2 \tag{13}$$

We can define an equivalent backscattering width ℓ as

$$\ell = \lim_{\rho\to\infty} 2\pi\rho\,\frac{S_r}{S_i}\bigg|_{\theta=\theta_i} \tag{14}$$

whence we obtain

$$\ell = k_0\left|\frac{I_0 Z_0}{2E_0}\right|^2\left|T(\theta_i)e^{-jk_0 d\sqrt{\epsilon_r-\sin^2\theta_i}}\right|^2 \tag{15}$$

It remains to determine the relation between the wire current and the incident electric field. The total electric field E_y on the wire surface at $\rho = a$ is equal to $Z'_w I_0$, where Z'_w denotes the wire impedance per unit length (for a perfectly conducting wire, $Z'_w = 0$). We have

$$\frac{I_0}{2\pi}\int_{-\infty}^{\infty}\left[B(k_x)e^{-jk_{zg}d}+C(k_x)e^{-jk_{zg}a}\right]dk_x + E_t(0,-d) = Z'_w I_0 \tag{16}$$

This equation is easily solved for the wire current. We find

$$I_0 = \frac{T(\theta_i)E_0 e^{-jk_0 d\sqrt{\epsilon_r-\sin^2\theta_i}}}{jk_0 Z_0\zeta_n} \tag{17}$$

in which the normalized impedance per unit length ζ_n is given by

$$\zeta_n = \frac{Z'_w}{jk_0 Z_0} + \frac{1}{4j}H_0^{(2)}(k_g a) + \frac{1}{2\pi}\int_{-\infty}^{\infty} e^{-2jk_{zg}d}\left(\frac{k_{zg}-k_{z0}}{k_{zg}+k_{z0}}\right)\frac{dk_x}{2jk_{zg}} \tag{18}$$

The scattering width ℓ is therefore

$$\ell = \frac{|T(\theta_i)|^4}{k_0|2\zeta_n|^2}\left|e^{-jk_0 d\sqrt{\epsilon_r-\sin^2\theta_i}}\right|^4 \tag{19}$$

In the limiting case where the wire is perfectly conducting and situated in free space, the scattering width reduces to

$$\ell \to \frac{4}{k_0|H_0^{(2)}(k_0 a)|^2} \tag{20}$$

or, since $k_0 a << 1$,

$$\ell \to \frac{4\pi^2}{k_0[4\ln^2(\gamma k_0 a/2) + \pi^2]} \tag{21}$$

in which $\gamma = 1.781\ldots$ is the exponential of Euler's constant.

Equivalent Impedance Per Unit Length of a Tunnel

The equivalent impedance per unit length of a cylindrical free-space region of radius a in a medium of relative permittivity ϵ_r is easily shown to be

$$Z'_w = \frac{jk_0 Z_0}{\pi(k_0 a)^2(\epsilon_r - 1)} \tag{22}$$

when $k_0 a$ is small compared to unity. To derive this result, consider the problem of plane-wave scattering from a cylindrical free-space region in a medium of relative permittivity ϵ_r. (The axis of the cylindrical region is taken to be the z-axis for this calculation.) When $k_0 a$ is small compared to unity, the electric field E_z just outside the cylinder is given by

$$E_{z>}(\rho) = E_0 J_0(k_g \rho) + A H_0^{(2)}(k_g \rho) \tag{23}$$

and inside the cylinder

$$E_{z<} = B J_0(k_0 \rho) \tag{24}$$

in which the constants A and B are to be determined. The magnetic field H_ϕ is obtained from

$$H_\phi(\rho) = \frac{1}{jk_0 Z_0}\frac{\partial E_z}{\partial \rho} \tag{25}$$

Making E_z and H_ϕ continuous at $\rho = a$ and solving for A, we obtain

$$A = E_0 \frac{k_g J_0(k_0 a) J_0'(k_g a) - k_0 J_0'(k_0 a) J_0(k_g a)}{k_0 J_0'(k_0 a) H_0^{(2)}(k_g a) - k_g J_0(k_0 a) H_0^{(2)'}(k_g a)} \tag{26}$$

The equivalent current is simply

$$I_{eq} = 2\pi a H_{\phi,sc}(a) = \frac{2\pi a}{jk_0 Z_0} A k_g H_0^{(2)'}(k_g a) \tag{27}$$

and the electric field at $\rho = a$ is

$$E_z(a) = E_0 J_0(k_g a) + A H_0^{(2)}(k_g a) \tag{28}$$

The equivalent impedance per unit length is

$$Z'_w = E_z(a)/I_{eq} \tag{29}$$

from which we obtain, substituting as appropriate and taking the limit as $k_0 a$ and $k_g a$ become small, the result given in eq. (22).

Numerical Results

The computation of the scattering width is straightforward. The normalized impedance per unit length ζ_n given in eq. (18) includes a known term for Z'_w, the Hankel function, and the

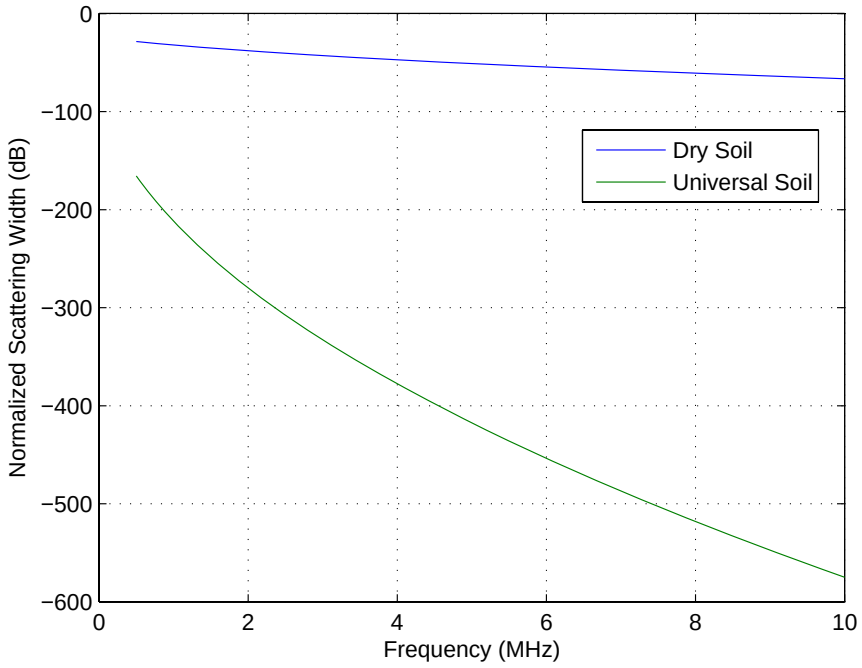

Figure 1: Normalized scattering width of PEC "tunnel" vs. frequency for very dry soil and universal soil. Soil parameters are $\epsilon_{ri} = 7$ and $\sigma_0 = 10^{-4}$ S/m for the very dry soil and $\epsilon_{ri} = 40$ and $\sigma_0 = 10^{-2}$ S/m for the Universal soil; the geometrical parameters are $a = 5$ meters, $d = 50$ meters, $\theta_i = 0$.

integral that represents the field reflected back to the wire by the air-ground interface. That integral can be written in the form

$$\mathcal{I}(k_0 d, \epsilon_r) = \frac{1}{2\pi} \int_{-\infty}^{\infty} e^{-2jk_{zg}d} \left(\frac{k_{zg} - k_{z0}}{k_{zg} + k_{z0}} \right) \frac{dk_x}{2jk_{zg}} = \frac{1}{2\pi} \int_0^{\infty} e^{-2k_0 d\sqrt{u^2-\epsilon_r}} \left(\frac{\sqrt{u^2-\epsilon_r} - \sqrt{u^2-1}}{\sqrt{u^2-\epsilon_r} + \sqrt{u^2-1}} \right) \frac{du}{\sqrt{u^2-\epsilon_r}} \quad (30)$$

The integral is now easily evaluated numerically.

We show some representative results in Figures 1 through 5. The scattering width of the tunnel is normalized by that of a PEC pipe of the same radius in free space and is plotted as a function of frequency or incidence angle. The burial depth is assumed to be 50 m and the tunnel radius is 5 m. The incidence angle is 0 degrees. The relative permittivity of the ground is expressed in terms of a high-frequency relative permittivity ϵ_{ri} and a low-frequency conductivity σ_0 as [1]

$$\epsilon_r = \left(\sqrt{\epsilon_{ri}} + \sqrt{\sigma_0 Z_0/(jk_0)} \right)^2. \quad (31)$$

Figures 1 and 2 compare the normalized scattering widths of a PEC "tunnel" and an air-filled tunnel vs. frequency for very dry soil and universal soil, respectively. We note that the normalized scattering widths decrease as frequency increases. Furthermore, we find that the

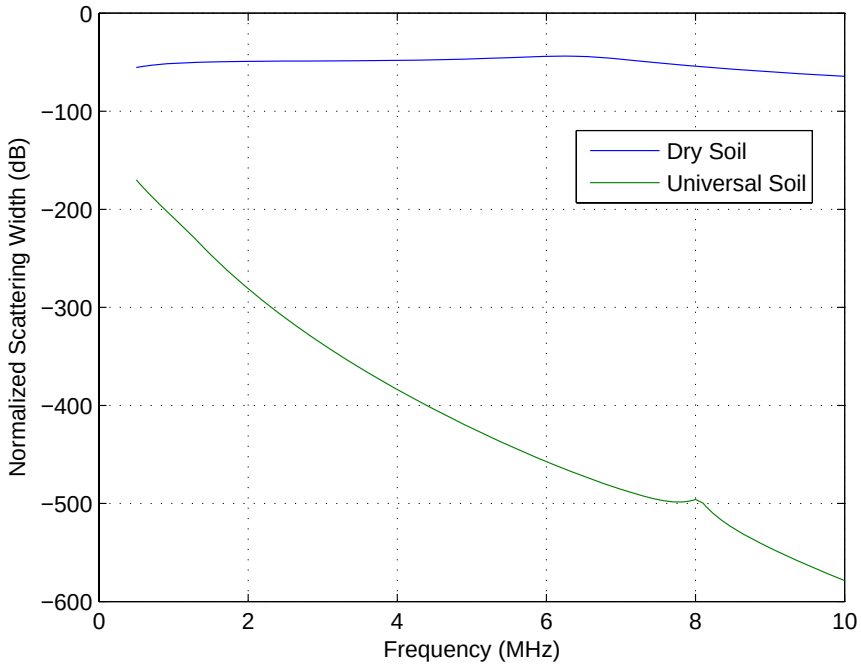

Figure 2: Normalized scattering width of air filled tunnel vs. frequency for very dry soil and universal soil. Soil parameters are $\epsilon_{ri} = 7$ and $\sigma_0 = 10^{-4}$ S/m for the very dry soil and $\epsilon_{ri} = 40$ and $\sigma_0 = 10^{-2}$ S/m for the Universal soil; the geometrical parameters are $a = 5$ meters, $d = 50$ meters, $\theta_i = 0$.

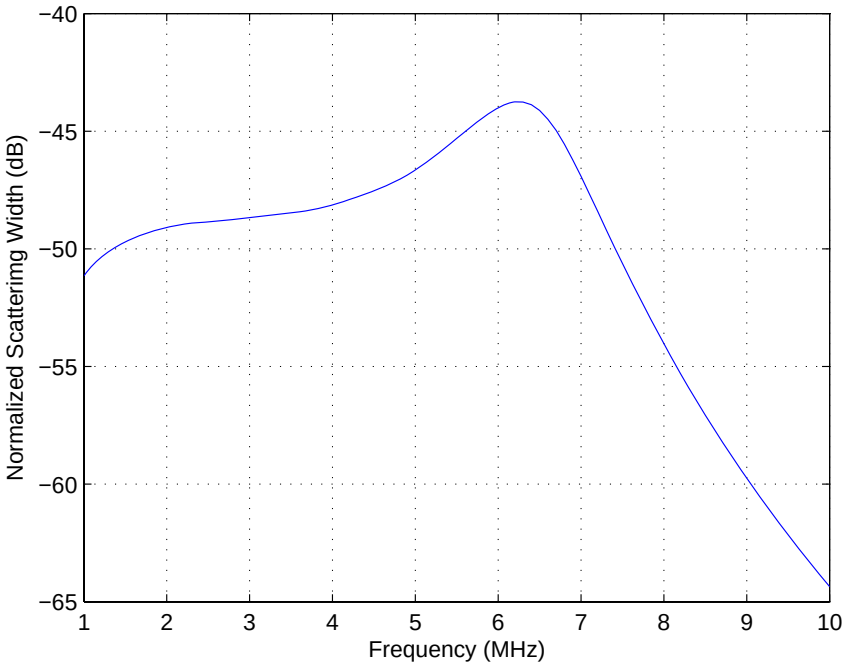

Figure 3: Normalized scattering width of air filled tunnel vs. frequency for very dry soil; soil parameters are $\epsilon_{ri} = 7$ and $\sigma_0 = 10^{-4}$ S/m; the geometrical parameters are $a = 5$ meters, $d = 50$ meters, $\theta_i = 0$.

normalized scattering widths drop rapidly as the soil moisture content increases. This means that it could be very difficult to find deeply buried underground targets as the soil moisture becomes large.

Figure 3 displays the dependence of the normalized scattering width of an air-filled tunnel on signal frequency for very dry soil.

Figures 4 and 5 depict the normalized scattering widths of a PEC "tunnel" and an air-filled tunnel vs. frequency for very dry soil and universal soil, respectively. Both demonstrate the property that the backscattered signal strengths decrease as the incidence angle becomes greater.

3 Rough-Surface Effects on Electromagnetic Scattering from a Tunnel in a Lossy Half-Space

In this section we discuss the reduction in coherent backscattered power when the interface between the upper air region and the lower dielectric region is rough.

The interface is modeled as a random-phase screen. The mean air-ground interface is located at $z = 0$; the region $z > 0$ is air and the region $z \leq 0$ is ground, with (generally complex) relative permittivity ϵ_r. The actual air-ground interface is the surface $z = \Delta(x, y)$. We assume that the random process $\Delta(x, y)$ is homogeneous in the wide sense, with expected value $\overline{\Delta(x, y)} = 0$ and variance $\overline{\Delta^2}$.

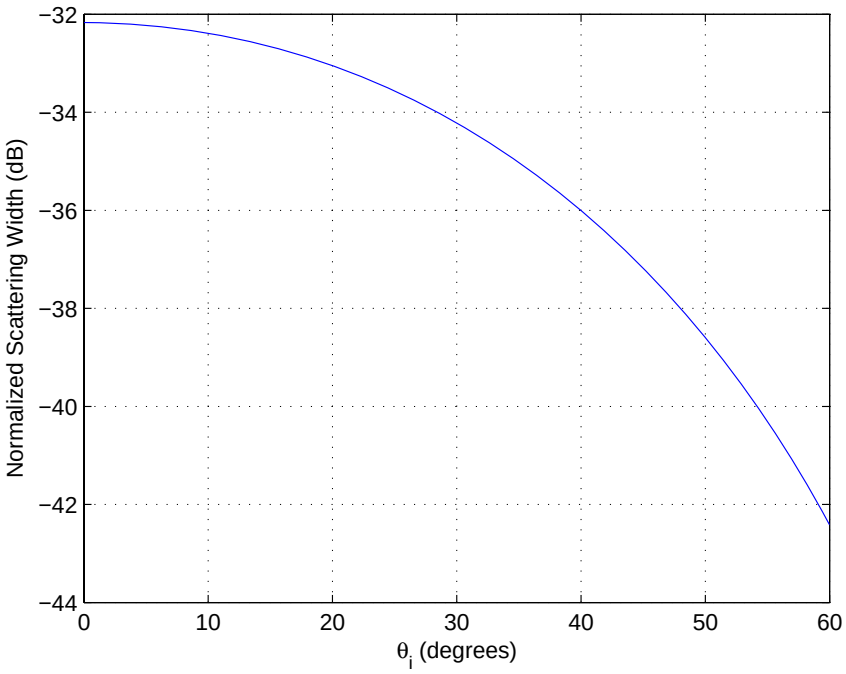

Figure 4: Normalized scattering width of PEC "tunnel" vs. incidence angle for very dry soil. Soil parameters are $\epsilon_{ri} = 7$ and $\sigma_0 = 10^{-4}$ S/m; $f = 1MHz$; the geometrical parameters are $a = 5$ meters, $d = 50$ meters.

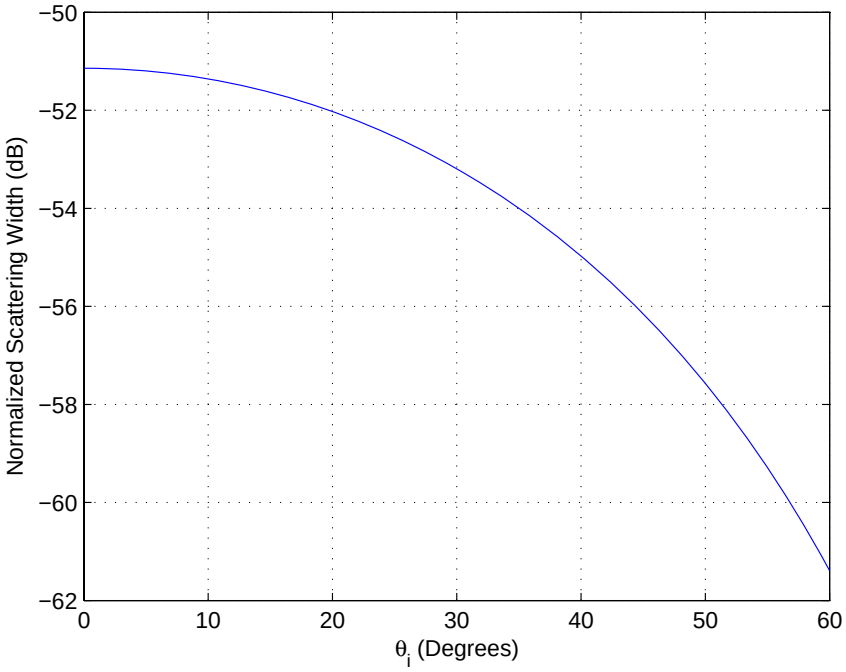

Figure 5: Normalized scattering width of air filled tunnel vs. incidence angle for very dry soil. Soil parameters are $\epsilon_{ri} = 7$ and $\sigma_0 = 10^{-4}$ S/m; $f = 1MHz$; the geometrical parameters are $a = 5$ meters, $d = 50$ meters.

Using this model, one can show (see, e.g., [2]) that the coherent amplitude of the electric field of a plane wave transmitted across the screen is reduced by the factor

$$F = \mathcal{E}\left\{e^{-jq(k_{x0},k_{y0})\Delta(x,y)}\right\} \tag{32}$$

in which k_{x0} and k_{y0} are the transverse propagation constants of the plane wave and the function q is given by

$$q(k_{x0},k_{y0}) = \Re\left\{\sqrt{k_0^2\epsilon_r - k_{x0}^2 - k_{y0}^2} - \sqrt{k_0^2 - k_{x0}^2 - k_{y0}^2}\right\} \tag{33}$$

with k_0 denoting the free-space wavenumber, and $\Re$ denotes the real part. If we further assume that the random process $\Delta(x,y)$ is Gaussian, it is easy to show that

$$F = e^{-q^2(k_{x0},k_{y0})\overline{\Delta^2}/2} \tag{34}$$

In the problem of backscattering from a buried target, the electromagnetic wave passes through the rough interface twice. Denoting the angle of incidence by θ and assuming that the incident plane wave is given by

$$E_{yi}(x,z) = E_0 e^{-jk_0(x\sin\theta - z\cos\theta)} \tag{35}$$

we have

$$q(k_{x0},k_{y0}) = k_0\Re\left\{\sqrt{\epsilon_r - \sin^2\theta} - \cos\theta)\right\} \tag{36}$$

The coherent backscattered electric-field amplitude is therefore reduced by the factor

$$F^2 = \exp\left[-k_0^2\overline{\Delta^2}\,\Re^2\left\{\sqrt{\epsilon_r - \sin^2\theta} - \cos\theta\right\}\right] \tag{37}$$

The backscattered power density, and thus the backscattering cross-section (or, in the case of a tunnel, the backscattering width), is reduced by the factor $|F|^4$. We remark that the phase-screen model is valid only when the phase shift imposed by the screen is small. The above result, therefore, is valid only for a "slightly rough" air-ground interface. The trend in the reduction of the backscattering cross-section, however, is clearly shown.

It should also be noted that a portion of the equivalent current induced on the buried tunnel results from reflection by the air-ground interface of the field that is radiated by the tunnel. Incorporating the rough-surface effects into the appropriate term in the normalized impedance per unit length ζ_n given in eq. (18), we have

$$\zeta_n = \frac{Z'_w}{jk_0Z_0} + \frac{1}{4j}H_0^{(2)}(k_g a) + \frac{1}{2\pi}\int_{-\infty}^{\infty} e^{-2jk_{zg}d}\exp\left\{-2\Re^2[k_{zg}]\overline{\Delta^2}\right\}\left(\frac{k_{zg}-k_{z0}}{k_{zg}+k_{z0}}\right)\frac{dk_x}{2jk_{zg}} \tag{38}$$

We remark that the reflection effect is very small over the parameter range of interest for the buried-tunnel problem.

Computations of the backscattering width are performed as in previous section, with the modification described above made in eq. (18), and the overall result multiplied by the factor $|F|^4$, as discussed in the foregoing.

Figures 6 and 7 compare the normalized scattering width of a PEC "tunnel" and an air-filled tunnel vs. frequency with and without the rough interface present. Figure 8 shows the normalized scattering width of an air-filled tunnel vs. the variance of the rough surface. These figures indicate that the roughness effects are very limited, even when the standard deviation of the roughness is large, since the frequency is so low.

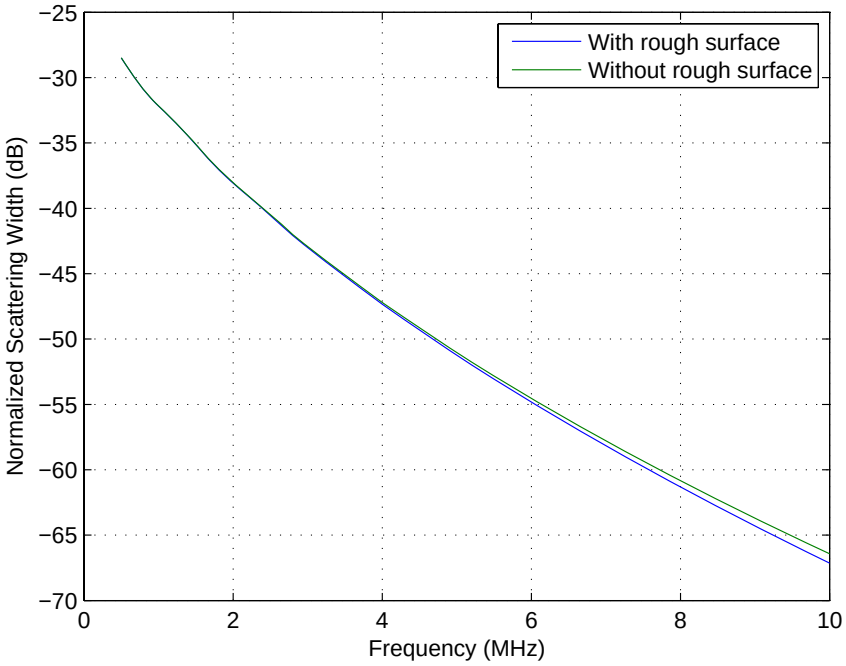

Figure 6: Normalized scattering width of PEC "tunnel" vs. frequency with and without the rough surface interface for very dry soil. Soil parameters are $\epsilon_{ri} = 7$ and $\sigma_0 = 10^{-4}$ S/m; the geometrical parameters are $a = 5$ meters, $d = 50$ meters, $\theta_i = 0$, variance $\overline{\Delta^2} = 1$ m^2.

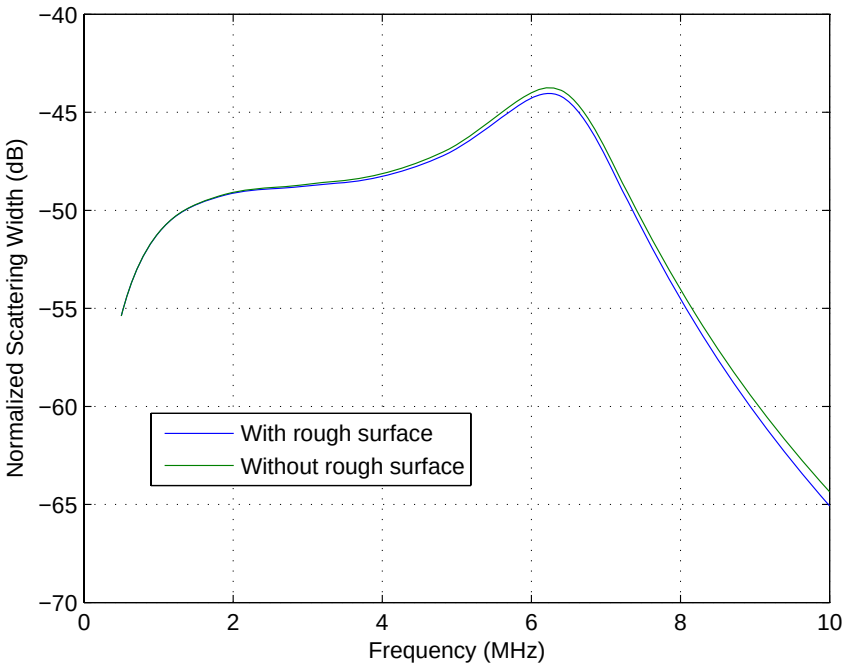

Figure 7: Normalized scattering width of air filled tunnel vs. frequency with and without the rough surface interface for very dry soil. Soil parameters are $\epsilon_{ri} = 7$ and $\sigma_0 = 10^{-4}$ S/m; the geometrical parameters are $a = 5$ meters, $d = 50$ meters, $\theta_i = 0$, variance $\overline{\Delta^2} = 1$ m^2.

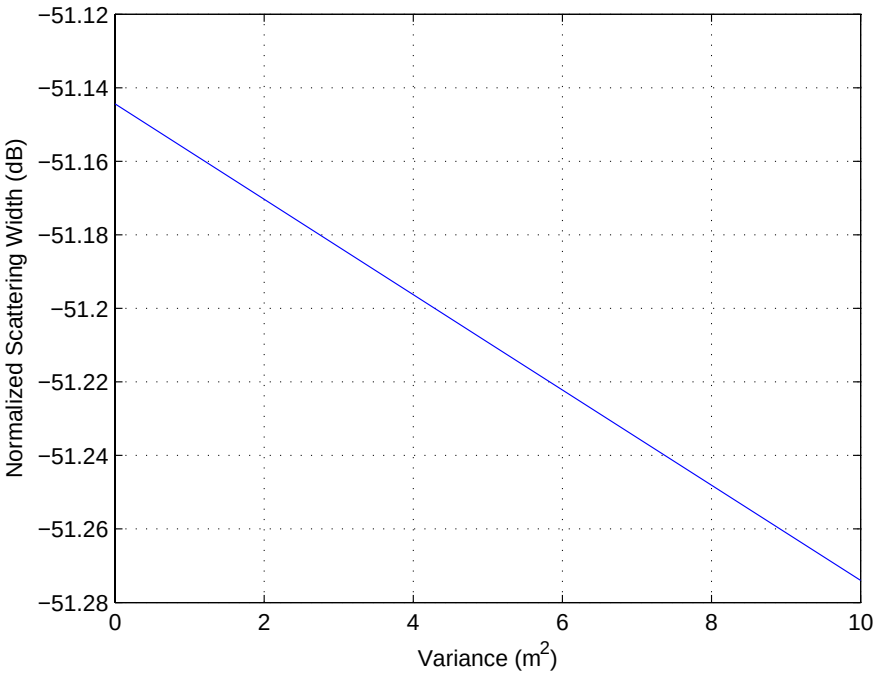

Figure 8: Normalized scattering width of air filled tunnel vs. the rough surface variance. Soil model is very dry soil: $\epsilon_{ri} = 7$ and $\sigma_0 = 10^{-4}$ S/m; $f = 1$MHz; the geometrical parameters are $a = 5$ meters, $d = 50$ meters, $\theta_i = 0$.

4 Electromagnetic Backscattering from Two Tunnels in a Lossy Half-Space

In this section, we consider electromagnetic backscattering from two tunnels in a lossy half-space. The tunnels are modeled as buried wires. The wires are located in the half-space $z < 0$, in which the relative permittivity is ϵ_r. The region $z > 0$ is free space. The wires are parallel to the y-axis and are located at positions $x = x_0, z = -d_0$ and $x = x_1, z = -d_1$. A perpendicularly-polarized plane electromagnetic wave is incident on the half-space from the free-space region $z > 0$. Proceeding as in Section 2, we find for the backscattered electric field in the far zone of the free-space region

$$E_{y>}(\rho,\theta) \sim -\frac{jk_0Z_0}{\sqrt{8\pi jk_0\rho}}\,T(\theta)e^{-jk_0\rho}\cdot \left[I_0e^{-jk_0(x_0\sin\theta+d_0\sqrt{\epsilon_r-\sin^2\theta})}+I_1e^{-jk_0(x_1\sin\theta+d_1\sqrt{\epsilon_r-\sin^2\theta})}\right] \quad (39)$$

where the currents I_0 and I_1 are to be determined.

The total electric field E_y in the lower medium is the sum of (i) the portion of the incident field that is transmitted into the lower medium, given by eq. (2); (ii) the electric field radiated by the current I_0 at $(x_0, -d_0)$ and reflected back into the lower medium by the interface at $z = 0$, as in eq. (5); and (iii) the electric field radiated by the current I_1 at $(x_1, -d_1)$ and reflected back into the lower medium by the interface at $z = 0$. The boundary condition to be imposed on the surface of each wire is that the electric field and the wire current be related by an equivalent impedance per unit length Z'_w via the two relations

$$E_y(x_0,-d_0) = Z'_{w0}I_0 \quad (40)$$

and

$$E_y(x_1,-d_1) = Z'_{w1}I_1 \quad (41)$$

in which, as was shown in Section 2, the impedances per unit length are given by

$$Z'_{w0} = \frac{jk_0Z_0}{\pi(k_0a_0)^2(\epsilon_r-1)} \quad (42)$$

$$Z'_{w1} = \frac{jk_0Z_0}{\pi(k_0a_1)^2(\epsilon_r-1)} \quad (43)$$

with a_0 and a_1 denoting the radii of the two tunnels.

The total electric field in the lower medium is given by

$$E_{yt}(x,z) = T(\theta_i)E_0e^{-jk_0(x\sin\theta_i-z\sqrt{\epsilon_r-\sin^2\theta_i})}+ \frac{I_0}{2\pi}\int_{-\infty}^{\infty}e^{-jk_x(x-x_0)}\left[B(k_x)e^{jk_{zg}(z-d_0)}+C(k_x)e^{-jk_{zg}|z+d_0|}\right]dk_x+ \frac{I_1}{2\pi}\int_{-\infty}^{\infty}e^{-jk_x(x-x_1)}\left[B(k_x)e^{jk_{zg}(z-d_1)}+C(k_x)e^{-jk_{zg}|z+d_1|}\right]dk_x \quad (44)$$

which we write in the form

$$E_{yt}(x,z) = E_t(x,z)+I_0e_{y0}(x,z)+I_1e_{y1}(x,z) \quad (45)$$

Imposing the conditions in eq. (40) and (41), we obtain the system of equations for the unknown currents

$$\begin{bmatrix} Z'_{w0} - e_{y0}(x_0, -d_0) & -e_{y1}(x_0, -d_0) \\ -e_{y0}(x_1, -d_1) & Z'_{w1} - e_{y1}(x_1, -d_1) \end{bmatrix} \cdot \begin{bmatrix} I_0 \\ I_1 \end{bmatrix} = \begin{bmatrix} E_t(x_0, -d_0) \\ E_t(x_1, -d_1) \end{bmatrix} \tag{46}$$

from which we obtain

$$I_0 = \frac{1}{D} \{[Z'_{w1} - e_{y1}(x_1, -d_1)]E_{yt}(x_0, -d_0) + e_{y1}(x_0, -d_0)E_{yt}(x_1, -d_1)\} \tag{47}$$

$$I_1 = \frac{1}{D} \{[Z'_{w0} - e_{y0}(x_0, -d_0)]E_{yt}(x_1, -d_1) + e_{y0}(x_1, -d_1)E_{yt}(x_0, -d_0)\} \tag{48}$$

with

$$D = [Z'_{w0} - e_{y0}(x_0, -d_0)][Z'_{w1} - e_{y1}(x_1, -d_1)] - e_{y0}(x_1, -d_1)e_{y1}(x_0, -d_0) \tag{49}$$

It is convenient to express the wire currents in terms of the incident electric field E_0 as $I_{0,1} = jk_0\ell_{0,1}E_0/(jk_0Z_0)$, where the definitions of the parameters $\ell_{0,1}$ (which have dimensions of length) are obvious from the foregoing. Then from (39), we have for the far-zone field backscattered into the upper region

$$E_{y>}(\rho, \theta) \sim -\frac{jk_0E_0}{\sqrt{8\pi jk_0\rho}} T(\theta_i)e^{-jk_0\rho} \cdot \left[\ell_0 e^{-jk_0(x_0 \sin\theta_i + d_0\sqrt{\epsilon_r - \sin^2\theta_i})} + \ell_1 e^{-jk_0(x_1 \sin\theta_i + d_1\sqrt{\epsilon_r - \sin^2\theta_i})}\right] \tag{50}$$

The backscattered power density, normalized by the incident power density, is therefore given by

$$\frac{S_r}{S_i} = \frac{1}{8\pi k_0\rho} |T(\theta_i)|^2 \cdot \left|k_0\ell_0 e^{-jk_0(x_0 \sin\theta_i + d_0\sqrt{\epsilon_r - \sin^2\theta_i})} + k_0\ell_1 e^{-jk_0(x_1 \sin\theta_i + d_1\sqrt{\epsilon_r - \sin^2\theta_i})}\right|^2 \tag{51}$$

and the equivalent backscattering width $\ell_{eq} = 2\pi\rho S_r/S_i$ is

$$\ell_{eq} = \frac{1}{4k_0} |T(\theta_i)|^2 \cdot \left|k_0\ell_0 e^{-jk_0(x_0 \sin\theta_i + d_0\sqrt{\epsilon_r - \sin^2\theta_i})} + k_0\ell_1 e^{-jk_0(x_1 \sin\theta_i + d_1\sqrt{\epsilon_r - \sin^2\theta_i})}\right|^2 \tag{52}$$

Computational Considerations

In this section we present formulas to aid in the numerical evaluation of the backscattered electric field and the equivalent backscattering width. We can express the normalized admittances in the form

$$jk_0\ell_0 = \frac{T(\theta_i)}{\mathcal{D}} \left[(\zeta_1 + \eta_{11})e^{-jk_0(x_0 \sin\theta_i + d_0\sqrt{\epsilon_r - \sin^2\theta_i})} - \eta_{10}e^{-jk_0(x_1 \sin\theta_i + d_1\sqrt{\epsilon_r - \sin^2\theta_i})}\right] \tag{53}$$

$$jk_0\ell_1 = \frac{T(\theta_i)}{\mathcal{D}} \left[(\zeta_0 + \eta_{00})e^{-jk_0(x_1 \sin\theta_i + d_1\sqrt{\epsilon_r - \sin^2\theta_i})} - \eta_{01}e^{-jk_0(x_0 \sin\theta_i + d_0\sqrt{\epsilon_r - \sin^2\theta_i})}\right] \tag{54}$$

in which

$$\mathcal{D} = (\zeta_0 + \eta_{00})(\zeta_1 + \eta_{11}) - \eta_{01}\eta_{10} \tag{55}$$

with

$$\zeta_{0,1} = \frac{Z'_{w0,1}}{jk_0Z_0} = \frac{1}{\pi(k_0a_{0,1})^2(\epsilon_r - 1)} \tag{56}$$

$$\eta_{00,11} = \frac{1}{\pi}\int_0^\infty \left(\frac{k_{zg}-k_{z0}}{k_{zg}+k_{z0}}\right) e^{-2jk_{zg}d_{0,1}} \frac{dk_x}{2jk_{zg}} + \frac{1}{4j} H_0^{(2)}(k_g a_{0,1}) \tag{57}$$

$$\eta_{01} = \eta_{10} = \frac{1}{\pi}\int_0^\infty \cos k_x(x_1 - x_0) \left(\frac{k_{zg}-k_{z0}}{k_{zg}+k_{z0}}\right) e^{-jk_{zg}(d_0+d_1)} \frac{dk_x}{2jk_{zg}} + \frac{1}{4j} H_0^{(2)}(k_g\sqrt{(x_1-x_0)^2+(d_1-d_0)^2}) \tag{58}$$

The integral terms in the expressions for η_{00} and η_{11} represent the field that is radiated from a wire and reflected back to the location of the same wire; the terms involving the Hankel functions represent the field radiated from a wire, evaluated at the surface of that wire. The integral terms in the expressions for η_{01} and η_{10} represent the field that is radiated from one wire and reflected back to the location of the other wire; the terms involving the Hankel functions represent the field radiated from one wire and evaluated at the surface of the other wire. The integrals are easily evaluated numerically.

It is of interest to determine the conditions under which the two tunnels can be resolved using observations of the equivalent scattering width. For simplicity, let us assume that the radii and the depths of the two tunnels are the same, equal to a_0 and d_0 respectively. Assume also that $x_0 = -s/2$ and $x_1 = s/2$ with s denoting the distance between the tunnel axes. Under these conditions, the equivalent backscattering width becomes

$$k_0\ell_{eq} = |T(\theta_i)|^4 \left|e^{-jk_0 d\sqrt{\epsilon_r - \sin^2\theta_i}}\right|^4 \left|\frac{(\zeta_0+\eta_{00})\cos(k_0 s\sin\theta_i) - \eta_{10}}{(\zeta_0+\eta_{00})^2 - \eta_{10}^2}\right|^2 \tag{59}$$

All dependence on the separation between the tunnel axes is contained in the last factor of the above equation: there is explicit dependence on s in the cosine function, and the factor η_{10} also depends on s. In the present instance, we have

$$\eta_{10}(s) = \frac{1}{\pi}\int_0^\infty \cos k_x s \left(\frac{k_{zg}-k_{z0}}{k_{zg}+k_{z0}}\right) e^{-2jk_{zg}d_0} \frac{dk_x}{2jk_{zg}} + \frac{1}{4j} H_0^{(2)}(k_g s) \tag{60}$$

for $s > 2a_0$.

It will be of interest to investigate the equivalent backscattering width as a function of incidence angle, frequency, tunnel radius and depth, and tunnel separation.

Figures 9, 10, and 11 depict the normalized scattering widths of air-filled tunnels vs. incidence angle for dry soil with the tunnels located at the same depth and different horizontal separation s. From Figure 9, we observe that the normalized scattering widths have no sidelobe in the incidence-angle range from -80° to 80° for $s < 0.26\lambda_0$. As s approaches $0.26\lambda_0$, the sidelobes begin to appear. This tells us that we might see an indication that two or more tunnels possibly exist from observations of the normalized scattering width. From Figure 10, we observe that the width of the main lobe becomes smaller and smaller as the separation s increases. From Figure 11, we observe that multiple sidelobes appear as the separation s becomes greater than one free space wavelength.

Figure 12 plots the normalized scattering width of two air-filled tunnels vs. incidence angle and frequency for very dry soil. We note that there is no sidelobe when the frequency is low (equivalent to small separation compared to free space wavelength). As frequency increases, the sidelobes appear (equivalent to large separation compared to wavelength). This plot confirms the conclusions drawn from three previous figures.

Figure 13 depicts the normalized scattering width of two air filled tunnels vs. incidence angle and horizontal separation for very dry soil. This figure further illustrates the results shown in Figures 9, 10, and 11.

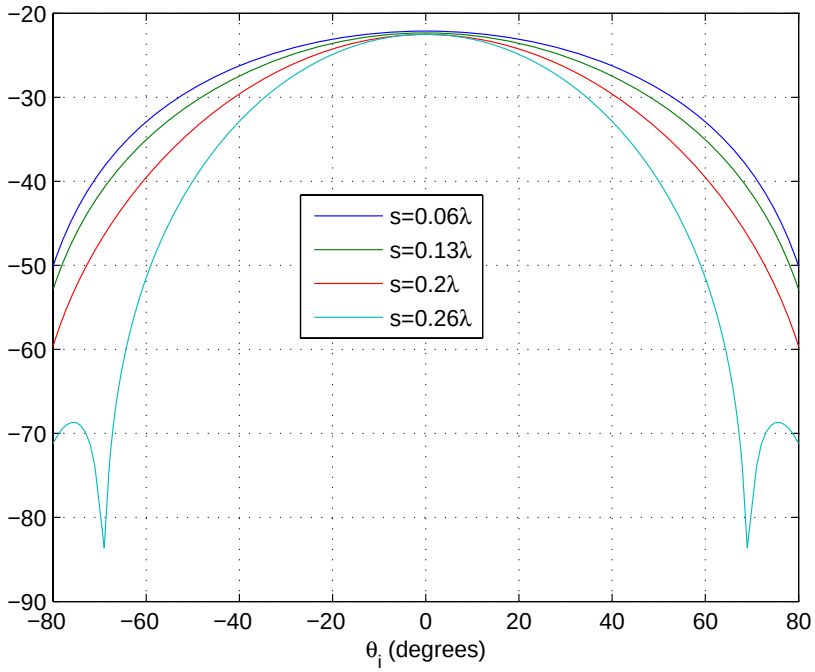

Figure 9: Normalized scattering width of air-filled tunnels vs. incidence angle for very dry soil with the tunnels located at the same depth and different horizontal separation s. Soil parameters are $\epsilon_{ri} = 7$ and $\sigma_0 = 10^{-4}$ S/m; $f = 1$MHz; the geometrical parameters are $a_0 = a_1 = 5$ meters, $d_0 = d_1 = 50$ meters.

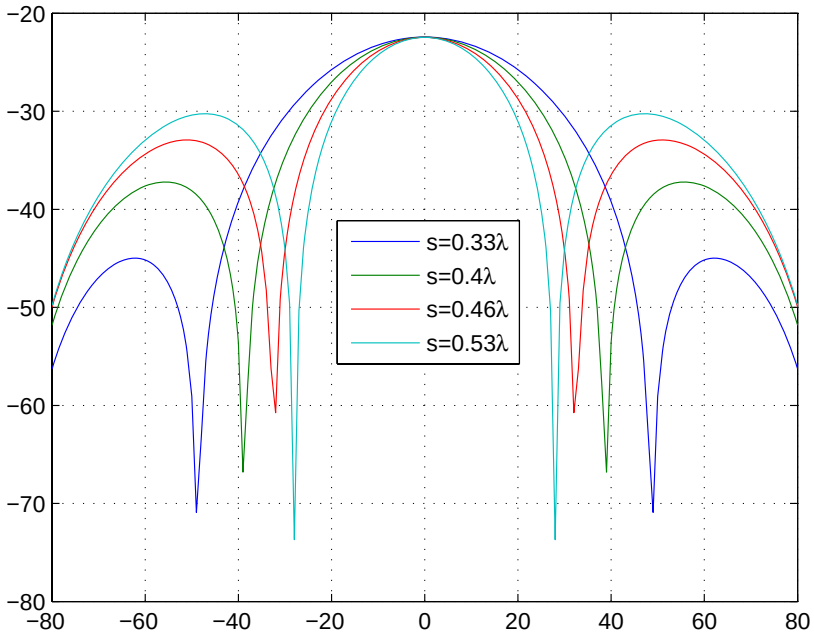

Figure 10: Normalized scattering width of air-filled tunnels vs. incidence angle for very dry soil with the tunnels located at the same depth and different horizontal separation s. Soil parameters are $\epsilon_{ri} = 7$ and $\sigma_0 = 10^{-4}$ S/m; $f = 1$MHz; the geometrical parameters are $a_0 = a_1 = 5$ meters, $d_0 = d_1 = 50$ meters.

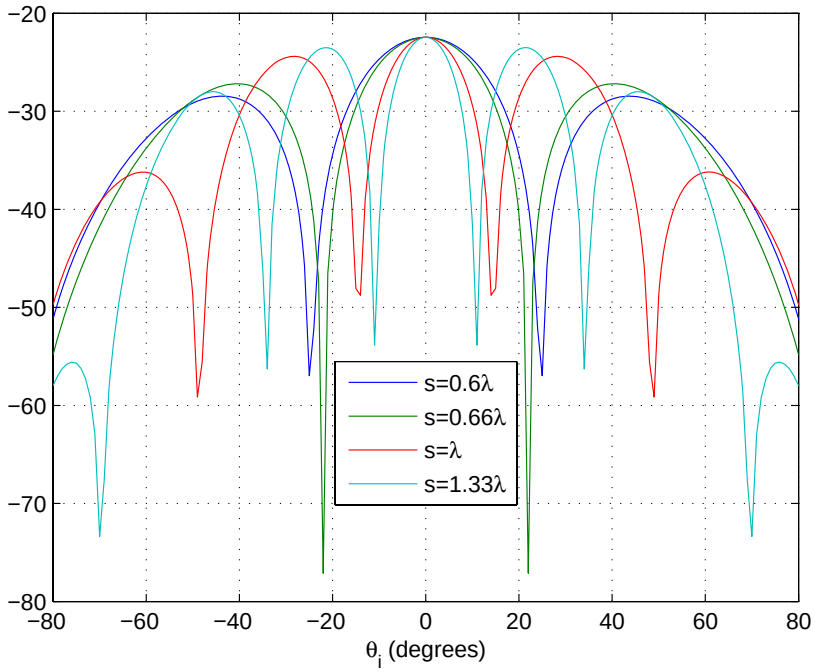

Figure 11: Normalized scattering width of air-filled tunnels vs. incidence angle for very dry soil with the tunnels located at the same depth and different horizontal separation s. Soil parameters are $\epsilon_{ri} = 7$ and $\sigma_0 = 10^{-4}$ S/m; $f = 1$MHz; the geometrical parameters are $a_0 = a_1 = 5$ meters, $d_0 = d_1 = 50$ meters.

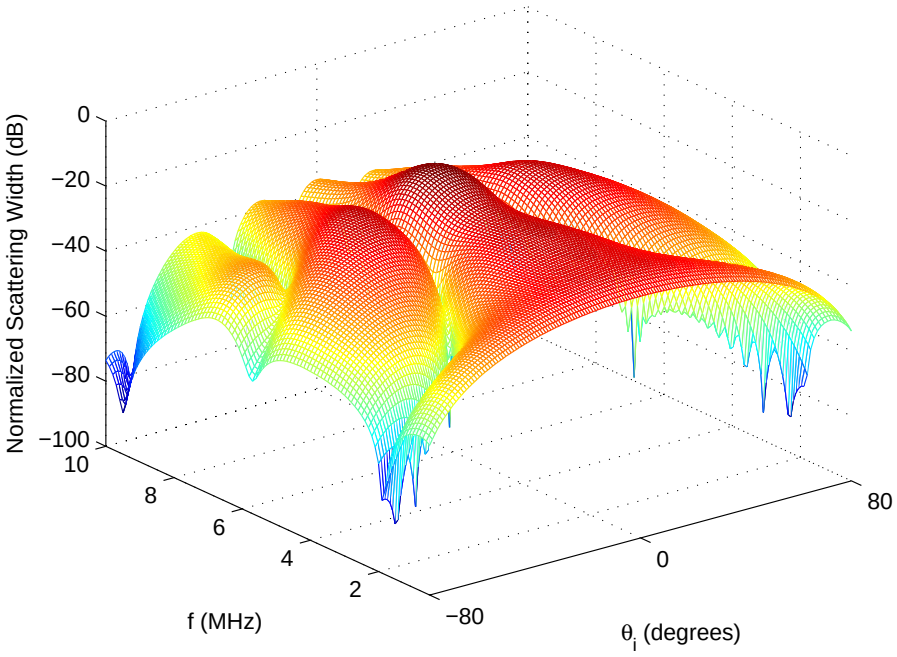

Figure 12: Normalized scattering width of air-filled tunnels vs. incidence angle and frequency for very dry soil. Soil parameters are $\epsilon_{ri} = 7$ and $\sigma_0 = 10^{-4}$ S/m; $f = 1$MHz; the geometrical parameters are the horizontal tunnel separation $s = 40$ meters, $a_0 = a_1 = 5$ meters, $d_0 = d_1 = 50$ meters.

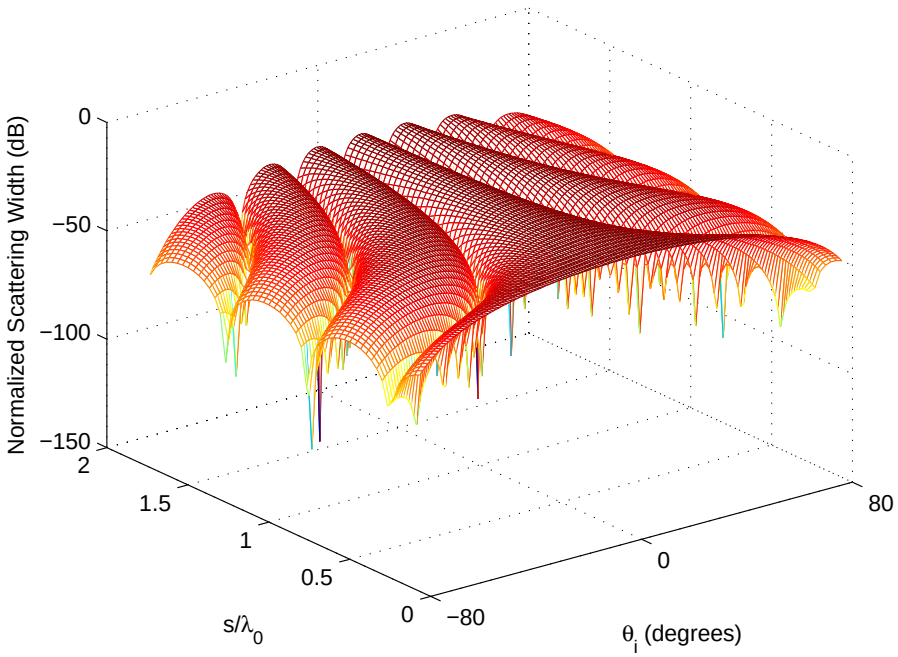

Figure 13: Normalized scattering width of air filled tunnels vs. incidence angle and horizontal separations for very dry soil. Soil parameters $\epsilon_{ri} = 7$ and $\sigma_0 = 10^{-4}$ S/m; $f = 1$ MHz; the geometrical parameters are $a_0 = a_1 = 5$ meters, $d_0 = d_1 = 50$ meters.

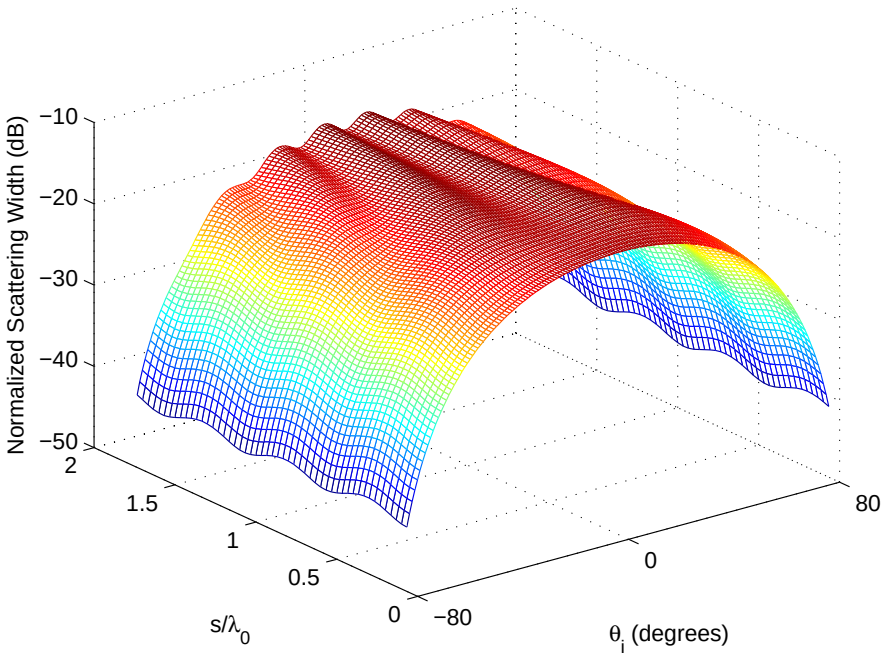

Figure 14: Normalized scattering width of air-filled tunnels vs. incidence angle and horizontal separations with different tunnel depths for very dry soil. Soil parameters are $\epsilon_{ri} = 7$ and $\sigma_0 = 10^{-4}$ S/m; $f = 1MHz$; the geometrical parameters are $a_0 = a_1 = 5$ meters, $d_0 = 70$ meters, $d_1 = 10$ meters.

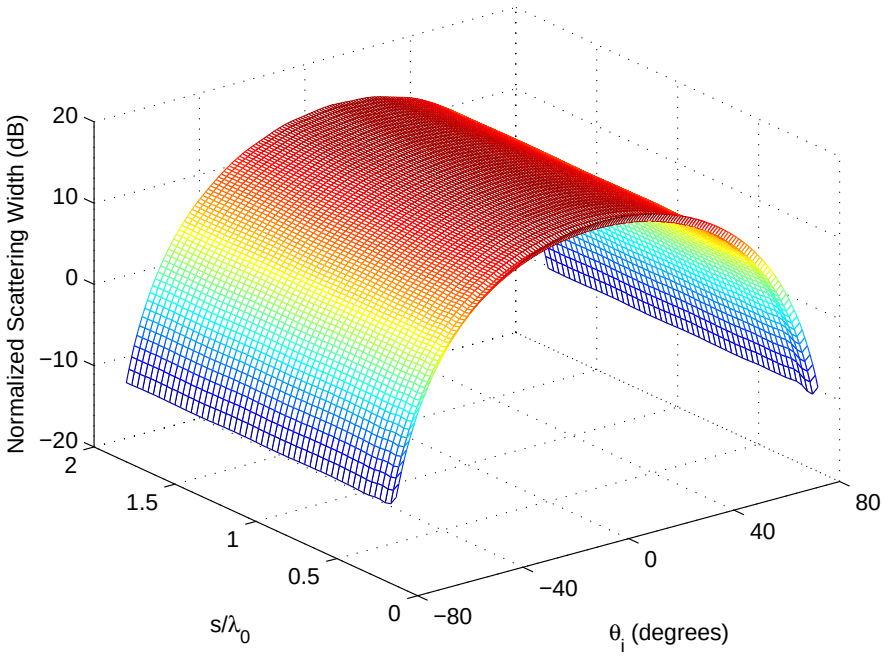

Figure 15: Normalized scattering width of air-filled tunnels vs. incidence angle and horizontal separations with different tunnel radius for very dry soil. The soil parameters are $\epsilon_{ri} = 7$ and $\sigma_0 = 10^{-4}$ S/m; $f = 1MHz$; the geometrical parameters are $a_0 = 25$ meters, $a_1 = 5$ meters, $d_0 = d_1 = 50$ meters.

Figure 14 shows the normalized scattering width of two air-filled tunnels vs. incidence angles and horizontal separations with different tunnel depths for very dry soil. The tunnel sizes are the same. We find that the sidelobes appear at relatively larger separation compared to the case in which the two tunnels are located at the same depth. Furthermore, the nulls are not as deep and sharp as in the case shown in Figure 13. This indicates that the interference is weak. We attribute this to fact that the scattered field strength contributed by the deeper tunnel is much less than that of the shallow one so that the scattering field strength contribution is dominated by the tunnel located closer to the air/earth interface. It is similar to the situation in which only one tunnel is present.

Figure 15 shows the normalized scattering width of two air-filled tunnels vs. incidence angle and horizontal separation with different tunnel radii for very dry soil. The tunnels are at the same depth. It is evident that there is no sidelobe; little or no interference is taking place. The larger tunnel dominates the scattering.

5 Concluding Remarks

In this report we have described the results of our initial investigations into problems of low-frequency electromagnetic backscattering from one or more tunnels located in a lossy half-space, in which the interface between the upper (air) and lower (ground) regions may be rough. The

fact that the tunnels are assumed to have a diameter that is small in comparison to the free-space wavelength allows us to model them as thin "wires" that are described by an equivalent impedance per unit length. Use of this approximation makes the computation of the backscattered field a relatively straightforward matter. We computed the backscattered electric field from one and two tunnels, for the case of the smooth interface between air and ground, for a range of parameters describing the signal frequency, tunnel depths and radii, incidence angles, and soil properties.

The inclusion of rough-surface effects was accomplished using the random phase-screen approximation for the rough interface. This approximation, which is applicable to the case in which the standard deviation of the surface roughness is small compared to the wavelength, allows us to quantify the reduction in the coherent power density transmitted through, or reflected by, a rough interface. We computed the backscattered field from a single tunnel for the case in which the air-earth interface was rough.

Further numerical investigations into the dependences of the equivalent backscattering length on the various parameters describing the problem can now easily be performed using the analytical results presented herein. In addition, it may be useful to consider problems for which the ground region comprises a topsoil and a subsoil layer, possibly with a rough interface between these two soil layers.

References

[1] M. A. Messier, "The propagation of an electromagnetic impulse through soil: influence of frequency dependent parameters," Tech. Rep. MRC-N-415, Mission Research Corporation, Santa Barbara, CA, 1980.

[2] Kendall F. Casey, "Rough-surface effects on subsurface target detection," Proceedings of SPIE, Vol. 4394, 2001.